 SDHM, vol.3, no.2, pp.69-79, 2007

Prediction of Crack Path Bifurcation under Quasi-Static Loading by the Cohesive Model

W. Brocks[1] **and I. Scheider**[1]

Abstract: Cohesive models are used for numerical crack extension analyses in order to predict the mechanical behavior of structures in cases of crack path bifurcation. Possible applications range from the macroscopic to the microscopic scale. As an example of applications to macroscopic engineering structures, simulations of a stiffened cylindrical shell under internal pressure are presented, where a skin crack may penetrate the rib or deviate. On the micro-scale, unit-cell calculation for a fiber-reinforced material is performed, where the fiber may debond or break.

Keyword: cohesive model, ductile tearing, crack bifurcation, cracked shell, metal matrix composite.

1 Introduction

Cohesive models are used for numerical crack propagation analyses on various length scales for several decades now. They are used as interfaces in finite element analyses, which represent the damage and failure properties of the material. As the crack can extend along the boundaries of solid elements, only, the crack path is predefined by the mesh Thus, predictions of arbitrary crack paths are either foredoomed or, at least, require an unreasonably high number of degrees of freedom, as cohesive surfaces have to be introduced at the boundaries of all solid elements in a meshed structure. However, interface elements can be advantageous for the numerical prediction of crack paths, if there is only a limited number of alternatives for the crack to extend, i.e. in bifurcation problems. Such problems play an important role in the frame of structural integrity analyses.

[1] GKSS Research Centre Geesthacht, Institute of Materials Research, Germany

Crack branching has been successfully modeled with cohesive elements mainly in brittle materials under dynamic loading. The present contribution addresses various different fracture mechanisms including ductile tearing of metals under quasi-static loading conditions. It aims at demonstrating the widespread applicability and versatility of cohesive models ranging from the macro- to the micro-scale. Two examples for predicting the mechanical behavior of structures in the presence of cracks are presented. At the macroscopic scale, the residual strength of a pressurized cylindrical shell with stiffeners and a one-bay crack, which may penetrate the stringer or deviate circumferentially along the skin, is calculated. Secondly, a unit-cell of a fiber-reinforced material is analyzed, where the fiber may debond or break. The latter is an example for an application at the microscale.

2 The Cohesive Model

2.1 Fundamentals

Dugdale (1960) and Barenblatt (1962) introduced a cohesive zone ahead of the crack tip in order to avoid the unrealistic infinite stress, which is characteristic for the stress intensity factor approach. Modern phenomenological cohesive models (Hillerborg et al., 1976, Needleman, 1987, 1990, Tvergaard and Hutchinson, 1992) describe various kinds of decohesion processes by a relation between surface tractions or cohesive stresses, $\sigma^T = \{\sigma_n, \sigma_t, \sigma_s\}$, having one normal and two tangential components and the material separation, $\delta^T = \{\delta_n, \delta_t, \delta_s\}$, where $\delta = [\mathbf{u}] = \mathbf{u}^+ - \mathbf{u}^-$ is the displacement jump over the interface. Cohesive zones are introduced in finite element meshes as surface elements at the boundaries of solid elements along pre-defined crack paths.

The phenomenological constitutive relation of the interface elements, the so-called cohesive or, more precisely, decohesion law, $\boldsymbol{\sigma} = \mathbf{f}(\boldsymbol{\delta})$, cannot be measured directly. The various functions for the decohesion behavior proposed and used in the literature (see overview by Brocks et al., 2003) have in common that they contain two characteristic parameters per crack opening mode, a cohesive strength, σ_c, and a critical separation, δ_c. The cohesive law represents the effective mechanical behavior due to the physical processes of material separation or fracture. For ductile materials, the relevant separation mechanism is micro-void nucleation, growth and coalescence, and the cohesive parameters can get a micromechanical interpretation (Brocks, 2005). For mode I ductile fracture, a rather versatile cohesive law,

$$\sigma_n(\delta_n) = \sigma_c \cdot \begin{cases} 2\left(\frac{\delta_n}{\delta_1}\right) - \left(\frac{\delta_n}{\delta_1}\right)^2 & \text{for } \delta_n \le \delta_1 \\ 1 & \text{for } \delta_1 < \delta_n \le \delta_2 \\ 2\left(\frac{\delta_n-\delta_2}{\delta_c-\delta_2}\right)^3 - 3\left(\frac{\delta_n-\delta_2}{\delta_c-\delta_2}\right)^2 + 1 & \text{for } \delta_2 \le \delta_n \le \delta_c \end{cases} \tag{1}$$

as proposed by Scheider (2001), is applied in the following, see Figure 1. It contains two additional shape parameters, δ_1 and δ_2. The interface elements are realized as user-defined element, UEL, in the FE code ABAQUS for 2D and 3D applications, and they were particularly adapted to plane stress and shell structures by incorporating the change of element thickness (Scheider and Brocks, 2005, Brocks and Scheider, 2006).

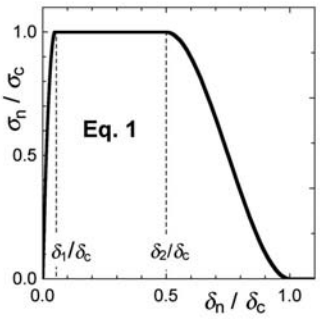

Figure 1: Cohesive law according to Eq. (1) for $\delta_1 = 0.05\ \delta_c$, $\delta_2 = 0.50\ \delta_c$.

The parameter δ_1 in Eq. (1) should be chosen as small as possible to obtain a high initial stiffness of the cohesive elements, as the deformation of the structure has to be dominated by the deformation of the solid elements. The parameter δ_2 allows for a variation between deformation controlled, $\delta_2 \to \delta_1$, and an abrupt stress release, $\delta_2 \to \delta_c$. Alternatively to δ_c, the mode-I energy-release rate or separation energy, Γ_c, which represents the area under the traction-separation law,

$$\Gamma_c = \int_0^{\delta_c} \sigma_n(\delta_n)\, d\delta_n = \sigma_c \delta_c \left(\frac{1}{2} - \frac{1}{3}\frac{\delta_1}{\delta_c} + \frac{1}{2}\frac{\delta_2}{\delta_c}\right), \tag{2}$$

can be introduced as a cohesive parameter. Estimates for the cohesive parameters in mode I fracture are the maximum true tensile stress at fracture of a notched tensile bar for the cohesive strength, σ_c, and the J-integral at crack initiation, J_i, for the separation energy, Γ_c, (Cornec et al., 2003). Note however, that the cohesive model is also applicable to the analysis of structures without cracks.

All cohesive models can be used for normal and tangential separation as well as for mixed mode loading. Unidirectional shear separation is treated in the same way as normal separation, Eq. (1). At combined normal and shear fracture, the shear damage will reduce the ductility in normal direction and vice versa

$$\sigma_n = f_n(\delta_n, \delta_t, \delta_s), \quad \sigma_{t,s} = f_{t,s}(\delta_n, \delta_t, \delta_s). \tag{3}$$

Various proposals for the mixed-mode coupling can be found in the literature (Tvergaard, 1990, Tvergaard and Hutchinson, 1993, Xu and Needleman, 1993, Camacho and Ortiz, 1996). Here, the approach of Scheider (2001) for simulating cup-cone fracture of a tensile bar is applied. A multiplicative decomposition of the interaction law between normal (mode I) and shear (mode II) separation,

$$\sigma_n = \sigma_c f(\delta_n) g(\delta_t), \quad \sigma_t = \sigma_c f(\delta_t) g(\delta_n), \tag{4}$$

is assumed, where $f(\delta)$ follows Eq. (1) and $g(\delta)$ is specified as

$$g(\delta) = 2\left(\frac{\delta}{\delta_c}\right)^3 - 3\left(\frac{\delta}{\delta_c}\right)^2 + 1. \tag{5}$$

If the normal separation, δ_n, reaches its final critical value, δ_{nc}, then $g(\delta_n) = 0$, i.e. no shear stresses can be transmitted by the interface, and this applies accordingly for the tangential separation.

2.2 Applications from macro to micro

Among various other applications, cohesive elements have in particular proven their capabilities for modeling crack extension in thin-walled shells and panels (Siegmund and Brocks, 2000, Roy and Dodds, 2001, Chabanet et al., 2003, Scheider et al., 2006). The two components of shear separation can then be identified as in-plane, mode II, and out-of-plane, mode III, i.e. $\sigma^T = \{\sigma_I, \sigma_{\mathrm{II}}, \sigma_{\mathrm{III}}\}$ and $\delta^T = \{\delta_I, \delta_{\mathrm{II}}, \delta_{\mathrm{III}}\}$. Plane stress analyses of shells and panels neglect the out-of-plane shear component, which nevertheless plays an important role in ductile fracture of thin panels. Even under remote mode I conditions, an extending crack generally inclines to an angle of 45° to the remote loading direction, Figure 2, thus inducing a local mode III field, a phenomenon known as "slant fracture" (Schroth et al., 1987, Kamat and Hirth, 1994, Mahgoub et al., 2003). Since cohesive elements in plane stress or shell finite element analyses are interfaces of line type, the inclined crack surface cannot be modeled with these elements and the material separation is therefore reduced to a fictitious mode I fracture. Due to this phenomenological description of the separation process, the cohesive parameters differ from those for a “real” mode I fracture.

Crack branching problems have been successfully modeled mainly for brittle materials under dynamic loading. Pioneering investigation on dynamic fracture applying the cohesive model have been published by Xu and Needleman (1994). To allow for arbitrary crack branching, cohesive surfaces have been introduced between all continuum elements. Xu and Needleman (1996) later presented an investigation on cracking at an interface between PMMA and aluminum under impact loading. Further studies on interfacial dynamic fracture applying viscoplastic constitutive equations were presented by Siegmund and Needleman (1997). Repetto et al. (2000) simulated fragmentation of a glass rod under impact loading. Ruiz et al. (2001) performed 3D simulations of tension-shear processes and mixed mode fracture in concrete.

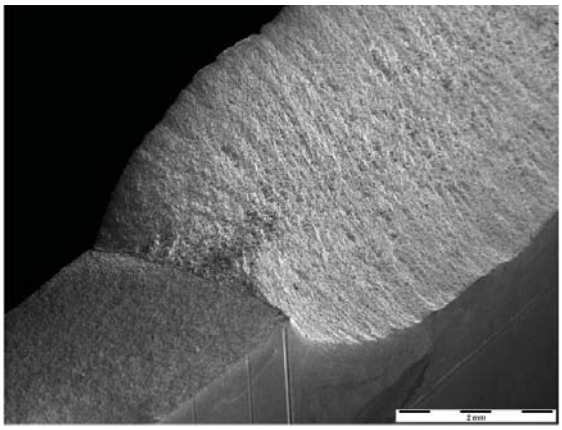

Figure 2: Slant fracture under remote mode I loading, material Al 5083.

Cohesive elements cannot only be used at a macroscale for predicting the structural behavior of components. They are also frequently used for analyzing damage mechanisms in the microstructure of materials. For these purposes, so-called representative volume elements (RVEs) are introduced, which are assumed to represent a typical material volume consisting of various constituents. Depending on the microstructure, RVEs have the size of a few mm^3 down to a few μm^3. The model proved successful for microcracking at grain boundaries of brittle ceramics (Zavattieri and Espinosa, 2001). Tijssens et al. (2001) analyzed an RVE of concrete on a mesolevel consisting of aggregates in a cement paste.

The smallest RVE of a microstructure is a unit cell, which may consist of a matrix containing a single inclusion, only. The propagation of cracks at fiber-matrix interfaces was modeled by Needleman (1990) and Tvergaard (1990, 1993, 1995). The initiation mechanisms of damage in ductile metals, namely particle cracking and debonding, were investigated by Steglich et al. (1999).

This fragmentary overview over the respective literature demonstrates the widespread applicability

and versatility of cohesive models ranging from structural integrity to micromechanical analyses.

3 Residual strength of aircraft fuselages

3.1 Problem Statement

The certification of airplanes requires a series of complex and expensive test procedures on components of different kinds, from specimens and single parts to the complete aircraft. Thus, the approval of new materials for use in aerospace industry as well as the implementation of optimized design represents an immense expense. Developing acknowledged methods for which some of these experiments can be replaced by numerical simulations is hence a big challenge.

Present-day aircraft design is based on a damage tolerance concept (Atluri, 1997; Broek, 1996; Kaplan and Wolff, 1996; Congourdeau and Journet, 2004), which acknowledges the existence of cracks and structural damage. The construction has to be designed in a way that any crack extension during service will not lead to catastrophic failure within the inspection intervals. The prediction of the residual strength of stiffened and un-stiffened thin-walled panels and shells in aircraft structures is an essential part of any damage tolerance analysis. Typical characteristics, which a respective failure assessment concept has to take into account, are (i) pronounced stable crack extension prior to failure and (ii) constraint effects and related issues, which make any application of standard test methods for fracture toughness impossible or too conservative.

Analytical and numerical methods have been specifically adapted to thin-walled structures, for instance R-curve approaches based on the crack tip opening displacement (CTOD) or the crack tip opening angle (CTOA), see Newman et al. (1999, 2003). In the following, cohesive elements are applied.

3.2 Analysis of a Stiffened Cylindrical Shell

Cylindrical shells with circumferential stiffeners under internal pressure may be regarded as simplified models of an aircraft fuselage. The following example examines crack extension and residual strength of a pressurized shell of diameter $2R = 200$ mm, width $2W = 200$ mm, skin thickness $t = 1$ mm, containing a one-bay crack located between two stringers, $a_0/W = 0.5$, see Figure 3.

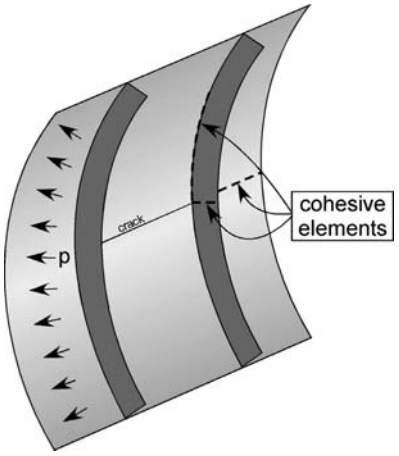

Figure 3: Stiffened cylinder with one-bay crack subject to internal pressure.

The FE model represents a 60° section of the total shell and accounts for symmetry, see Figure 4.

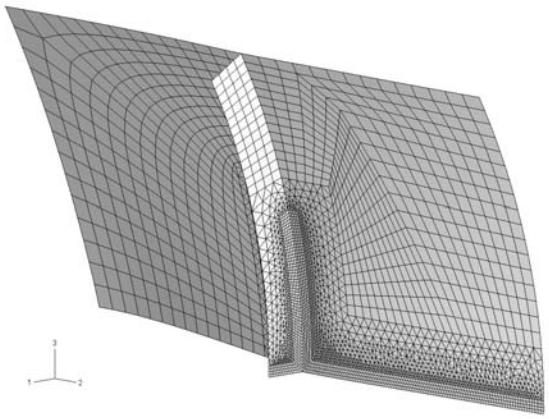

Figure 4: FE-model (quarter section) of the pressurized cylinder with crack.

The material is an aluminum alloy Al 6056 T78, which is considered as potential replacement of Al 2024, an alloy traditionally used for airplane fuselages. The material data and model parameters summarized in Table 1 have been deter-

mined in a broad study of the strength and toughness properties of welded panels by Nègre et al. (2005). The shape parameters of the cohesive law were chosen as $\delta_1/\delta_c = 0.01$ and $\delta_2/\delta_c = 0.05$.

Table 1: Material and model parameters for Al 6056 T78

Young's modulus	E [GPa]	70
yield strength	σ_Y [MPa]	302
hardening exponent	n [-]	0.67
cohesive strength (normal)	σ_c [MPa]	550
critical separation (normal)	δ_c [mm]	0.073
cohesive energy (normal)	Γ_c [J/m^2]	20.5

The cohesive model offers some variability in the potential direction of crack extension, as cohesive elements may be placed along various paths. In the present example, the locations of cohesive elements allow for crack extension in three directions, along a surface line of the skin, through the stringer and in circumferential direction along the stringer. The stringer thickness has been varied between t = 1.3 mm and 2.4 mm. The objective of this parameter study was to find out whether the crack continues extending in its original direction and thus ruptures the stringer or deviates and extends in circumferential direction along the stringer without penetrating it. Respective effects have been found on real structures.

The load-displacement curves for three values of stringer thickness, t, namely 1.3, 1.8 and 2.4 mm, are shown in Figure 5. The crack extension starts shortly below maximum load, i.e. residual strength. The latter increases remarkably, when the stringer thickness changes from 1.3 mm to 1.8 mm. At the same time, the stability characteristics of the load-deformation behavior alter. Whereas there is a smooth maximum for t = 1.3 mm, the pressure vs. CTOD curve decreases steeply after its maximum, that means structural failure will occur abruptly. No significant further increase of maximum load is observed for t > 1.8 mm. The increase of structural strength corresponds to a change of the crack path. For a stringer thickness of 1.3 mm the crack extends in its original direction in the shell structure and through the stringer, see Figure 6a. For stringer thicknesses of 1.8 mm and higher, the crack deviates at the stringer and extends circumferentially along the stringer without cutting it, see Figure 6b.

In addition to the effect of the stringer stiffness, which was studied here, one could also investigate the bonding strength of the stringer to the skin. In this case, the circumferential propagation of the crack would mean that the stringer peels off, which can actually be observed in tests.

Though no experimental data are available for validation, the broadly based experimental and numerical study of crack extension on C(T) and M(T) specimens by Scheider et al. (2006) documents the significance of the parameter studies performed on the shell structures. In addition to its predictive capabilities the excellent numerical performance of the cohesive model favors its application for predicting the residual strength of components like aircraft fuselages.

4 Damage of Metal Matrix Composites

4.1 Damage Mechanisms

Metal matrix composites (MMCs) with light metal matrices find increasing applications in transportation engineering, especially in the automotive industry, for example, partially fiber-reinforced pistons and hybrid reinforced crankcases in passenger cars and truck engines, and particle-reinforced brake discs for trucks, motorcycles, and passenger cars. The full potential of these materials can only be achieved, however, if accurate and reliable predictions of the constitutive behavior including the failure mechanisms under different loading and environmental conditions can be made. The reinforcing effect of short fibers can be attained only if there is a significant stress transfer from the matrix to the fibers (Kelly and Tyson, 1965). Therefore, the interface between fiber and matrix plays an important role.

Failure of fiber-reinforced components is generally preceded by an accumulation of different types of internal damage. Failure mechanisms on the micromechanical scale include: reinforcement (fiber, particle or flake) fracture, interfacial debonding and matrix damage. They vary with

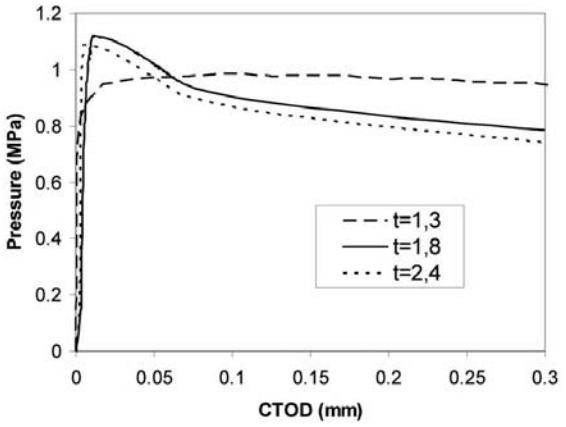

Figure 5: Pressure vs. crack-tip opening displacement for a stiffened cylindrical shell containing a one-bay crack, effect of stringer thickness.

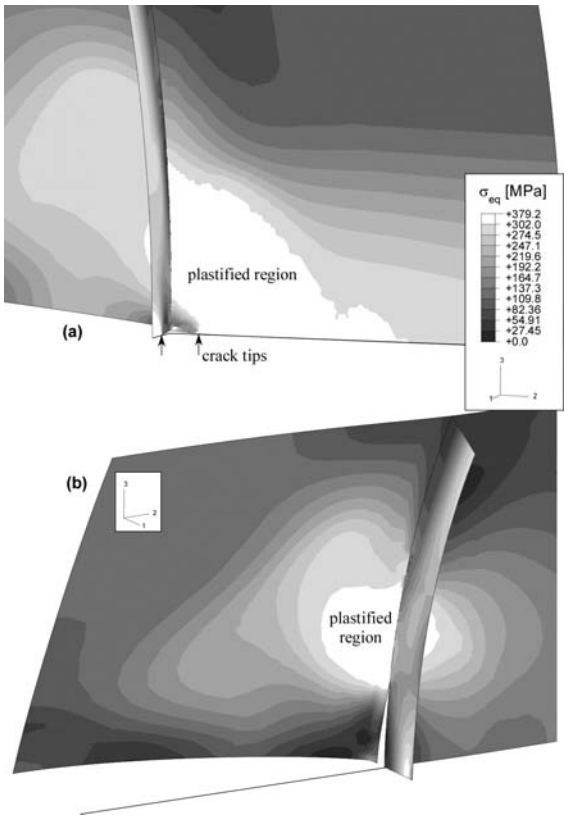

Figure 6: Crack extension in the pressurized cylindrical shell, effect of stringer thickness on crack path: (a) t = 1.3 mm, (b) t = 1.8 mm.

the type of loading and depend on the properties of the constituents. Cohesive elements are a valuable means of studying the interaction of the various mechanisms and the effects of varying parameters.

4.2 Unit Cell Model of a Metal-Matrix Composite

The present study investigates a composite of a Ti6 Al4 V matrix with SiC fibers. It is idealized as a periodic array of cylindrical unit cells of length L_c = 2 mm and radius R_c = 1 mm, each containing a longitudinally aligned fiber of length L_c = 1 mm and radius R_f = 50 μm. The spherical cylinder shown in Figure 7 is a simplification of a volume filling hexagon cylinder allowing for simple axisymmetric calculations.

The cell is loaded by uniaxial tension. In the initial unloaded state, the fiber is under compression

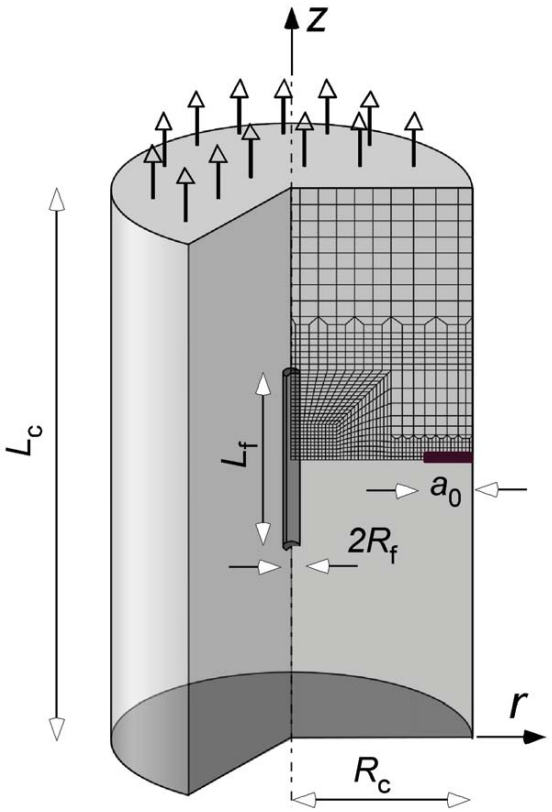

Figure 7: Cylindrical unit cell model of a metal-matrix composite.

resulting from the processing: Due to the different thermal expansion coefficients in fiber and matrix, the stresses in the fiber raise up to 2000 MPa, which is considered in the simulation by a thermal step with a temperature decreasing from 770°C to 20°C. The residual stresses have a significant effect on the fiber debonding characteristics and hence the overall mechanical behavior (Thionnet and Renard, 1998). In particular, Dinters et al. (1996) showed that the shear stresses at the interface are such that debonding occurs already after cooling. In the present configuration, the residual stresses will postpone the failure of the fiber and the interface, since the residual stresses countervail the applied external tensile loading.

The properties of the elasto-plastic matrix and the elastic fiber are taken from Jin et al. (2002) and summarized in Table 2.

Table 2: Material parameters for Ti 6 Al 4 V matrix and SiC fibers

		Matrix	Fiber
Young's modulus	E [GPa]	11.7	469
yield strength	σ_Y [MPa]	907	-
thermal expansion coefficient	$10^6\ \alpha[\mathrm{K}^{-1}]$	11.2	4.0

The matrix has a circumferential crack of depth a_0 = 0.1 mm in the center plane. The crack will extend in radial direction towards the fiber, where it may cut the fiber or bifurcate in z-direction and detach the fiber from the matrix. Cohesive elements are introduced at the fiber-matrix interface and at the symmetry plane, z = 0, both in the fiber and in the matrix, to model interface failure, fiber failure and matrix failure, respectively. The fiber–matrix interface elements are endowed with a normal strength and a shear strength and follow the mixed-mode criterion of Eq. 4. The cohesive properties summarized in Table 3 are more or less estimates used for a numerical parameter study. The failure strength, σ_c, of the fiber is provided by Jin et al. (2002), the fiber-matrix shear strength from Zeng et al. (2002). The shape parameters of the cohesive law are chosen as δ_1/δ_c = 0.001 and δ_2/δ_c = 0.10.

Table 3: Cohesive properties of the fiber, the matrix and the fiber-matrix interface

	σ_c [MPa]	Γ_c [kJ/m^2]	δ_c [mm]
fiber debonding (normal)	1000	0.55	0.001
fiber debonding (tangential)	450	0.25	0.001
fiber breaking (normal)	4450	2.45	0.001
matrix cracking (normal)	1100	12.10	0.020

Because of symmetry, only one half of the unit cell is meshed in the finite element model. The symmetry conditions are realized by the following boundary conditions,

$$\begin{aligned} u_r(0,z) &= 0, \quad 0 \le z \le L_c/2 \\ u_z(r,0) &= 0, \quad 0 \le r \le (R_c - a_0) \end{aligned} \tag{6}$$

Periodicity of the unit cells requires that the boundaries remain straight,

$$\begin{aligned} u_r(R_c/2,z) &= u_r(R_c/2,0), \quad 0 \le z \le L_c/2 \\ u_z(r,L_c/2) &= u_z(0,L_c/2), \quad 0 \le r \le R_c/2 \end{aligned} \tag{7}$$

Loading of the cell occurs displacement controlled at the upper surface, i.e. $u_z(0,L_c/2)$ is prescribed. The unit cell is subjected to uniaxial tension in the present case, i.e. $u_r(R_c/2,0)$ is not constrained. Biaxial tension would increase the stress triaxiality and affect the failure modes, of course.

In order to study the effect of the fiber geometry on the damage mechanisms occurring during loading and the final failure, the fiber diameter has been varied between 100 μm and 300 μm, where all cohesive parameters remained unchanged.

The overall mechanical behavior of the fiber-matrix aggregate, i.e. load $F = 2\pi \int_0^{R_c} \sigma_{zz}(r)\, r\, dr$ vs relative elongation, $2u_z/L_c$, appears to be rather

insensitive to changes of the fiber diameter. Particularly, maximum load and fracture strain do not vary significantly. A close look on the respective curves however reveals small pop-in events near maximum load for fiber diameters $2R_f \geq 150\ \mu$m, which actually indicate a change of the failure mechanism.

The effects of damage evolution become more distinct by plotting the fiber stresses, σ_{zz}, at $z = 0$, $r = 0$ vs. matrix crack opening, COD = $2u_z(r = R_c/2,\ z = 0)$. Figure 8 displays the results for two fiber diameters, namely $2R_f = 120\ \mu$m and $2R_f = 200\ \mu$m.

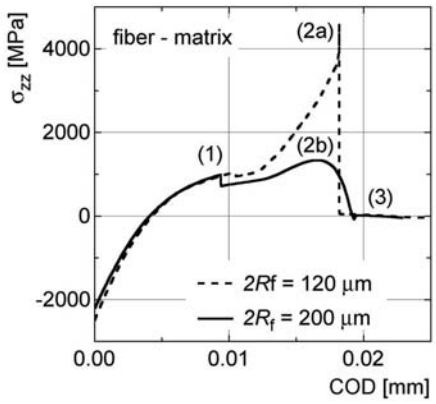

Figure 8: Fiber stresses, σ_{zz}, at $z = 0$ vs. matrix crack opening, COD, for varying fiber diameters.

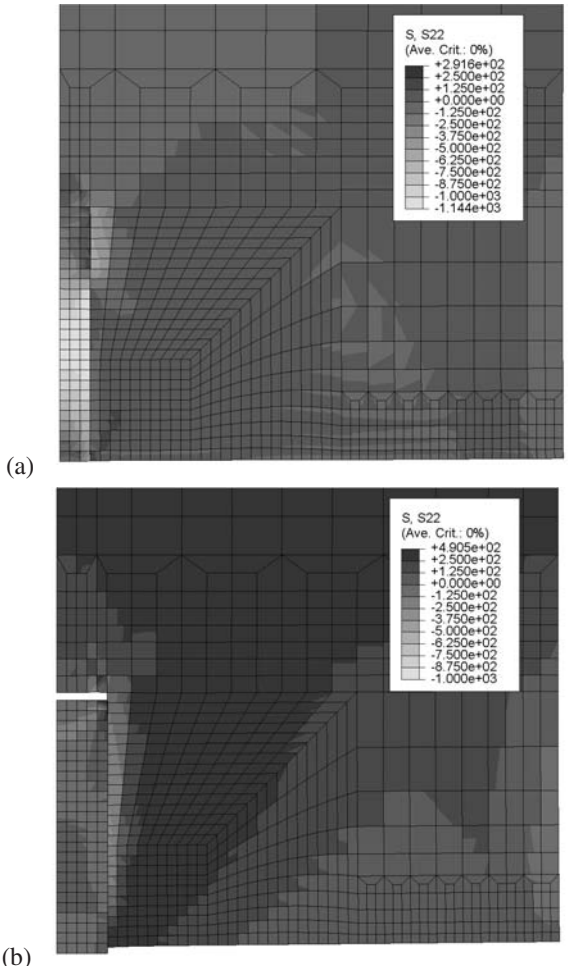

Figure 9: Isocontours of stresses σ_{zz} at final failure for (a) $2R_f = 120\ \mu$m, (b) $2R_f = 200\ \mu$m.

The fiber is subject to compressive residual stresses in the beginning which results from processing. Damage of the aggregate starts with detachment of the fiber at its top face (1) followed by some tangential debonding at the interface in the early stages of loading and growing matrix crack. Total failure requires complete breaking of the matrix in all cases, but the fiber behaves differently depending on its diameter. If the fiber diameter is small, $2R_f = 120\ \mu$m, final failure occurs by fiber breakage (2a), when the stresses reach the fiber strength of $\sigma_c = 4450$ MPa. For the larger fiber diameter, $2R_f >= 200\ \mu$m, final failure occurs by complete fiber debonding from the matrix (2b) and the normal stresses are limited by the tangential fiber debonding strength of 450 MPa due to local equilibrium. For both mechanisms, fiber stresses decrease to zero at total failure (3). The respective stress state in the cell is displayed in Figure 9.

The residual stress state is strongly inhomogeneous in the thinner fiber, Figure 9a. Though the stresses σ_{zz} at $z = 0$ and $z = L_f/2$ are nearly zero, significant compressive stresses of up to 1100 MPa occur in-between as the fiber is still bonded to the matrix in this area. At the already debonded upper third of the fiber compressive stresses occur in the matrix.

The stresses σ_{zz} in the thicker fiber are predominantly zero, Figure 9b. The gap between the fiber's top surface and the matrix and the opening of the matrix crack is clearly visible. Residual stresses in the matrix change from compression

close to the fiber to tension apart.

The example demonstrates the potential of cohesive models to analyze phenomena and mechanisms of damage evolution in heterogeneous materials. It provides physically significant parameters for characterizing microstructural features like debonding or fracture strength of inclusions.

5 Summary and Conclusions

The cohesive model has proven its ability to predict crack extension and crack path bifurcation on various length scales. Possible applications range from the assessment of residual strength of components down to the analysis of damage phenomena in heterogeneous materials. Though only simulations of cracked structures have been presented here, cohesive models do not rely on the existence of an initial crack in general. This is an important advantage compared to fracture mechanics concepts.

Suitable meshing is crucial however to realize the actual crack path. Other methods like continuum damage models or XFEM are better suited for simulations of completely arbitrary and continuously changing crack paths. Particularly in three-dimensional models, the approach of introducing cohesive elements between all continuum elements may lead to an unreasonably high number of elements. In addition, the initial elastic stiffness of the cohesive law becomes an important and often critical issue.

Cohesive interfaces are advantageous, when there is a limited number of possibilities for the crack to grow. The model is numerically stable for large crack extensions, it is not subject to any pathological mesh dependence like damage models and it provides physically meaningful parameters for characterizing strength and toughness of materials.

References

Ananth, C.R.; Voleti, S.R.; Chandra, N. (1989): Effect of fibre fracture and interfacial debonding on the evolution of damage in metal matrix composites. *Composites Part A*, vol. 29, pp. 1203-1211.

Atluri, S.N. (1997): *Structural Integrity and Durability*. Tech Science Press, Forsyth, GA, USA.

Barenblatt, G.I. (1962): The mathematical theory of equilibrium cracks in brittle fracture. *Adv Appl Mech*, vol. 7, pp. 55-129.

Brocks, W. (2005): Cohesive strength and separation energy as characteristic parameters of fracture toughness and their relation to micromechanics. *Structural Integrity and Durability*, vol.1, pp. 233-244.

Brocks, W.; Cornec, A.; Scheider, I. (2003): Computational aspects of nonlinear fracture mechanics. In: I. Milne, O. Ritchie, B. Karihaloo, B (eds.): *Comprehensive structural integrity. Fracture of materials from nano to macro*, vol. 3, Elsevier, Oxford, 127-209.

Brocks, W.; Scheider, I. (2006): Cohesive elements for thin-walled structures. *Comp Mat Sci*, vol. 37 pp. 101-109.

Broek, D. (1996): Concepts of fracture control and damage tolerance analysis. *ASM International*, vol. 19, pp. 410-419.

Camacho, G.T.; Ortiz, M. (1996): Computational modelling of impact damage in brittle materials. *Int J Solids Struct*, vol. 33, pp. 2899-2938.

Chabanet, O.; Steglich, D.; Besson, J.; Heitmann, V.; Hellmann, D.; Brocks, W. (2003): Predicting crack growth resistance of aluminium sheets. *Comp Mat Sci*, vol. 26, pp. 1-12.

Congourdeau, F.; Journet, B. (2004): Damage tolerance of fuselage welded stiffened panels. *Proc. 22nd Symp. Int. Committee on Aeronautical Fatigue (ICAF)*, May 2003, Lucern (Switzerland), pp. 361-384.

Cornec, A.; Scheider, I.; Schwalbe, K.H. (2003): On the practical application of the cohesive model. *Engng Fract Mech*, vol. 70, pp. 1963-1987.

Dinters, J.; Peters, P.W.M.; Hemptenmacher, J. (1996): Finite element modeling of the push-out test for SiC fibre-reinforced titanium alloys. *Composites Part A*, vol. 27, pp. 749-753.

Dugdale, D.S. (1960): Yielding of steel sheets containing slits. *J Mech Phys Solids*, vol. 8, pp.

100-104.

Hillerborg, A.; Modeer, M.; Petersson, P.E. (1976): Analysis of crack formation and crack growth in concrete by means of fracture mechanics and finite elements. *Cement Concrete Res*, vol. 6, pp. 773-782.

Kamat, S.V.; Hirth, J.P. (1994): A mixed mode I/III fracture toughness correlation. *Scripta Metall Mater*, vol. 30, pp. 145-148.

Kaplan, M.P.; Wolff, T.A. (1996): Life extension and damage tolerance of aircraft. *ASM International*, vol. 19, pp. 557-565.

Kelly, A.; Tyson, W.R. (1965): Tensile properties of fibre-reinforced metals. *J Mech Phys Solids,* vol. 13, pp. 329-350.

Mahgoub, W.; Deng, X.; Sutton, M.A. (2003): Three-dimensional stress and deformation fields around flat and slant cracks under remote Mode I loading conditions. *Engng Fract Mech,* vol. 70, pp. 2527-2542.

Needleman, A. (1987): A continuum model for void nucleation by inclusion debonding. *J Appl Mech*, vol. 54, pp.525-531.

Needleman, A. (1990): An analysis of decohesion along an imperfect interface. *Int J Fract*, vol. 42, pp. 21-40.

Negre, P.; Steglich, D.; Brocks, W. (2005): Crack extension at an interface: prediction of fracture toughness and simulation of crack path deviation. *Int J Fract*, vol. 134, pp. 209-229.

Newman, J.C.; Bigelow, C.A.; Dawicke, D.S. (1999): Finite-element analyses and fracture simulation in thin-sheet aluminum alloy, In: *Durability of Metal Aircraft Structures, Proc. Int. Workshop on Structural Integrity of Aging Airplanes*, pp. 167-.

Newman, J.C.; James, M.A.; Zerbst, U. (2003): A review of the CTOA/CTOD fracture criterion. *Engng Fract Mech*, vol. 70, pp. 371-385.

Repetto, E.A.; Radovitzky, R.; Ortiz, M. (2000): Finite element simulation of dynamic fracture and fragmentation of glass rods. *Comput Meth Appl Mech Eng*, vol. 183, pp. 3-14.

Roy, Y.A., Dodds, R.H. (2001): Simulation of ductile crack growth in aluminium panels using 3-D surface cohesive elements. *Int J Fract*, vol. 110, pp. 21-45.

Ruiz, G.; Pandolfi, A.; Ortiz, M. (2001): Three-dimensional cohesive modeling of dynamic mixed-mode fracture. *Int J Numer Meth Eng*, vol. 52, pp. 97-120.

Scheider, I. (2001): Simulation of cup-cone fracture in round bars using the cohesive zone model. In: K.J.Bathe (ed.): *Proc. 1st MIT Conf. Computational Fluid and Solid Mechanics*, pp. 460-462.

Scheider, I.; Brocks, W. (2005): Simulation of crack propagation and failure in shell structures using the cohesive model. In: Ramm, E, Wall, WA, Bletzinger, KU, Bischoff, M (eds.): *Proc 5th Int. Conf. Computation of Shell and Spatial Structures*. Salzburg (Austria).

Scheider, I.; Schödel, M.; Brocks, W.; Schönfeld, W. (2006): Crack propagation analyses with CTOA and cohesive model: Comparison and experimental validation. *Engng Fract Mech*, vol. 73, pp. 252-263.

Schroth, J.G.; Hirth, J.P.; Hoagland, R.G.; Rosenfield, A.R. (1987): Combined Mode I-Mode III fracture of a high strength low-alloy steal. *Metall Trans A*, vol. 18A, pp. 1061-1072.

Siegmund, T.; Brocks, W. (2000): Simulation of ductile crack growth in thin aluminum alloys. In: G.R. Halford, J.P. Gallagher (eds.) *31st Nat Symp Fatigue and Fracture Mechanics*, Cleveland (OH, USA), ASTM STP 1389, pp. 475 - 485.

Siegmund, T.; Needleman, A. (1997): A numerical study of dynamic crack growth in elastic-viscoplastic solids. *Int J Solids Struct*, vol. 34, pp. 769-787.

Steglich, D.; Siegmund, T.; Brocks, W. (1999): Micromechanical modelling of damage due to particle cracking in reinforced metals. *Comp Mat Sci*, vol. 16, pp. 404-413.

Su X.F.; Chen, H.R.; Kennedy, D.; Williams, F.W. (1999): Effect of interphase strength on the damage modes and mechanical behaviour of metal-matrix composites. *Composites Part A*, vol. 30, pp. 257-266.

Thionnet, A.; Renard, J. (1998): Multi-scale analysis to determine fibre/matrix debonding cri-

teria in SiC/Titanium composites with and without consideration of the manufacturing residual stresses. *Composite Sci Techn*, vol. 58, pp. 945-955.

Tijssens, M.G.A.; van der Giessen, E.; Sluys, L.J. (2000): Modeling of crazing using a cohesive surface methodology. *Mech Mat*, vol. 32, pp. 19-35.

Tvergaard, V. (1990): Effect of fibre debonding in a whisker-reinforced metal. *Mat Sci Eng A*, vol. 125, pp. 83-151.

Tvergaard, V. (1993): Model studies of fibre breakage and debonding in a metal reinforced by short fibres. *J Mech Phys Solids*, vol. 41, pp. 1309-1326.

Tvergaard, V. (1995): Fibre debonding and breakage in a whisker-reinforced metal. *Mat Sci Eng A*, vol. 190, pp. 215-222.

Tvergaard, V.; Hutchinson, J.W. (1992): The relation between crack growth resistance and fracture process parameters in elastic-plastic solids. *J Mech Phys Solids*, vol. 40, pp. 1377-1397.

Tvergaard, V.; Hutchinson, J.W. (1993): The influence of plasticity on mixed mode interface toughness. *J Mech Phys Solids*, vol. 41, 1119-1135.

Xu, X.; Needleman, A. (1993): Void nucleation by inclusion debonding in a crystal matrix. *Modell Simul Sci Eng*, vol. 1, pp.111-132.

Xu, X.; Needleman, A. (1994): Numerical simulations of fast crack growth in brittle solids. *J Mech Phys Solids*, vol. 42, pp.1397-1434.

Xu, X.; Needleman, A. (1996): Numerical simulations of dynamic crack growth along an interface. *Int J Fract*, vol. 74, pp. 289-324.

Zavattieri, P.D.; Espinosa, H.D. (2001): Grain level analysis of crack initiation and propagation in brittle materials. *Acta Mater*, vol. 49, pp. 4291-4311.

Zeng, W.D.; Peters, P.W.M.; Tanaka, Y. (2002): Interfacial bond strength and fracture energy at room and elevated temperature in titanium matrix composites (SCS-6/Timetal 834). *Composites: Part A*, vol. 33, pp. 1159-1170.